# Nondispersing wave packets

H. Maeda and T. F. Gallagher
*Department of Physics, University of Virginia, Charlottesville, Virginia 22904-0714, USA*
(Received 7 December 2006; published 22 March 2007)

A nondispersing Rydberg wave packet can be made by applying a weak, linearly polarized field at the Kepler frequency of a Rydberg atom. The field phase locks the electron's motion to the microwave field, and the wave packet retains its spatial localization for times in excess of a microsecond. The electron's orbital oscillation leads to an oscillating dipole, which can either oscillate in phase or out of phase with the applied microwave field, creating wave packets analogous to Trojan and anti-Trojan wave packets described theoretically. Our observations can be described in both quantum mechanical and classical terms.

DOI: 10.1103/PhysRevA.75.033410 PACS number(s): 32.80.Rm, 32.80.Qk

## I. INTRODUCTION

One of the great successes of quantum mechanics was to explain the fact that the optical spectrum of the hydrogen atom is composed of discrete spectral lines matching the energy spacings between quantized energy levels, not a continuous spectrum as might be expected from classical mechanics [1]. While the success of quantum mechanics was beyond question, the notion of a theory based on stationary wave functions instead of moving particles was unsettling, and to show the connection between the classical and quantum theories Schrödinger constructed wave packets, coherent superpositions of harmonic oscillator wave functions in which the probability density moved just as a classical particle would [2].

The case Schrödinger chose, the harmonic oscillator, is unique in having evenly spaced levels, so that once created, the wave packet lasts indefinitely. In reality most physical systems are not composed of evenly spaced levels, and wave packets constructed in such systems disperse in time. This problem was pointed out to Schrödinger by Lorentz [3], and the fact that atomic Rydberg wave packets would disperse was noted by Brown [4].

Wave packets remained theoretical constructs until the advent of mode-locked lasers, which have allowed their formation and detection. Atomic Rydberg radial wave packets have been made by creating coherent superpositions of different $n$ states of the same $\ell$. We follow the usual convention that $n$, $\ell$, and $m$ are the principal, orbital-angular momentum, and azimuthal angular-momentum quantum numbers. In a radial wave packet the probability of finding the electron oscillates radially in and out at the $\Delta n=1$, or Kepler frequency in the early stage of its oscillating behavior [5,6]. Molecular vibrational and rotational wave packets have been created as well [7,8]. Prior to the wave-packet experiments the essential elements of time-domain spectroscopy were demonstrated in quantum-beat experiments [9,10]. However, in these experiments the number of quantum states was typically small enough that dispersion of the energy spacings was not an issue. Shortly after the first radial Rydberg wave-packet experiments [11] it became clear that the dispersion in the level spacings dephased the wave packets after only a few orbits, and routes to the formation of longer-lived wave packets were explored [12–15].

One approach to making nondispersing wave packets is to use the Stark states of the same $n$ and $m$, which in hydrogen are uniformly spaced to first order in the electric field. In any other atom but hydrogen the levels are not evenly spaced, even to first order. More important, the energy spacing between levels is entirely due to the external field, making these wave packets very susceptible to dephasing by field inhomogeneities. In fact, such Stark wave packets are not longer lived than ordinary radial wave packets [12]. A fruitful route to the production of a nondispersing wave packet has been to add a weak field oscillating at the Kepler, or orbital frequency of the Rydberg electron. The first proposals were based on the use of circularly polarized fields [13] (and later with a combination of a circularly polarized field and a magnetic field [14,15]), but the experimental realizations have been with linearly polarized fields, both monochromatic and trains of pulses [16,17]. Previously we reported the production of nondispersing Rydberg wave packets with a monochromatic, linearly polarized microwave field [16]. Here we describe more extensive experiments and compare our observations to the results of classical and quantum calculations.

This paper is organized in the following manner. First, we recall the origin of dispersion in Rydberg wave packets and present a simple physical picture of how a microwave field can be used to form a nondispersing wave packet. We then describe our experimental approach and observations. Finally, we compare our observations to quantum and classical models.

## II. DISPERSION IN RYDBERG WAVE PACKETS AND NONDISPERSING WAVE PACKETS

The origin of dispersion in radial Rydberg wave packets, and the one-dimensional wave packets we consider here is in the energy-level structure. The energy $W_n$ of a state of principal quantum number $n$ is given by [18]

$$W_n = -\frac{1}{2n^2}. \tag{1}$$

We use atomic units unless specified otherwise. The time-dependent wave function $\psi_n(z,t)$ is given by the product of a spatial wave function and a phase factor, i.e.,

 

$$\psi_n(z,t) = \phi_n(z)e^{-iW_n t}, \tag{2}$$

where the spatial function $\phi_n(z)=zR_n(z)$, in which $R_n(z)$ is a hydrogen $n\ell$ radial function of $\ell=0$. A wave packet has a wave function that is a coherent superposition of wave functions of several $n$ states, i.e.,

$$\Psi(z,t) = \sum_n a_n \phi_n(z)e^{-iW_n t}, \tag{3}$$

and the probability density of finding the electron at position $z$ at time $t$ is given by

$$|\Psi(z,t)|^2 = \sum_{nn'} a_n a_{n'}^* \phi_n(z)\phi_{n'}^*(z)e^{-i(W_n - W_{n'})t}. \tag{4}$$

From Eq. (4) it is apparent that motion of the probability density comes entirely from the $n' \neq n$ cross terms of Eq. (4), and the frequency of the motion occurs at the frequency differences between the levels, a notion familiar from quantum-beat experiments.

If we differentiate Eq. (1) we find

$$\frac{dW_n}{dn} = \frac{1}{n^3}, \tag{5}$$

so the energy spacing between the levels is $1/n^3$. If the wave packet is composed of only five states or so the spacings between adjacent $n$ levels is approximately constant and equal to $1/\bar{n}^3$, where $\bar{n}$ is the central $n$ of the wave packet. If the spacing between adjacent levels was exactly $1/\bar{n}^3$ then all the beat frequencies present in Eq. (4) would be harmonics of $1/\bar{n}^3$ and the motion would be perfectly periodic with no dispersion or spatial spreading of the wave packet.

The $\Delta n$ spacings are not constant since

$$\frac{d^2W_n}{d^2n} = -\frac{3}{n}\left(\frac{1}{n^3}\right). \tag{6}$$

For example, at $n=60$ the frequency decreases by 5% with each increase in $n$ of one, so a wave packet containing five states has a 20% variation in beat frequencies and disperses in about five orbits. The orbits rephase, forming revivals of the wave packet [19], but eventually, usually in tens of orbits, the coherence of the wave packet disappears, and there is no detectable motion of the electron's probability distribution.

The essential notion of making a nondispersing wave packet is most easily understood if we consider circular states $|m|=\ell=n-1$. In a circular state the electron probability is a ring in the $x-y$ plane centered on the ionic core. It is radially localized in a trough formed by the centrifugal $\ell(\ell+1)/2r^2$ and the Coulomb $-1/r$ potentials. There is no azimuthal localization since the potential has no dependence on $\phi$ (where $\tan\phi=y/x$). If we apply a circularly polarized microwave field, which rotates in the $x-y$ plane at the Kepler frequency, we destroy the $\phi$ symmetry. In particular, the potential in which the electron is trapped has a low point, which rotates around the ionic core at the Kepler frequency, as shown in Fig. 1. Intuitively, the electron is likely to be localized in the low point. In a frame rotating with the microwave field the electron is trapped in the static potential well with its minimum at the low point. An electron localized at the lowest point of the well is exactly synchronized to the microwave field. If its energy is higher, it oscillates about the minimum, and the oscillation corresponds to the electron's orbital motion oscillating between leading and lagging the microwave field.

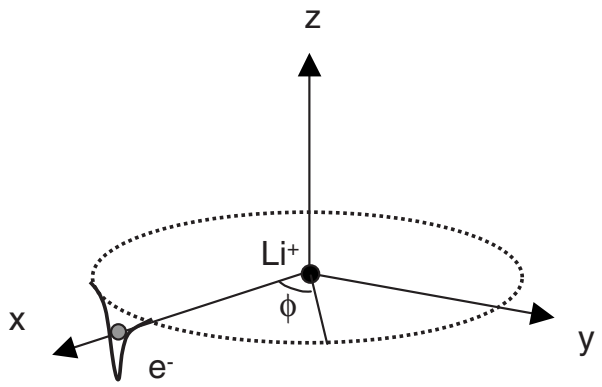


FIG. 1. With no microwave field the electron in a circular state is trapped in the trough of the combined centrifugal and Coulomb potential. The location of the minimum of the potential is shown by the broken line. There is no reason for the electron to be at any particular value of $\phi$. When the microwave field rotating in the $x$-$y$ plane is added the potential is distorted at the instant the field is in the $-x$ direction. There is now a potential well with a minimum on the $+x$ axis ($\phi=0$), as shown by a solid line. The electron has its lowest energy at this point, and remains in this well as the field rotates at a frequency near the natural orbital frequency of the electron.

In the laboratory frame the atom has a rotating dipole $\mu$, which is parallel to and synchronous with the rotating microwave electric field. This configuration is the one having the lowest energy. There are other stable configurations, and, in fact, the electron can be stable on the opposite side of the atom, where there is a potential hill. In this case the rotating atomic dipole is antiparallel to and synchronous with the microwave field. These two types of states have been termed Trojan and anti-Trojan wave packets [13,20]. They are analogous to the stable magnetic substates with different projections of magnetic moment on the magnetic field observed in the Stern-Gerlach experiment.

A linearly polarized microwave field at the Kepler frequency also leads to nondispersing wave packets in which the electron's motion is nearly linear and in the direction of the microwave field [21]. In this case the most stable states are the highest-energy states in which the atomic dipole $\mu$ oscillates exactly out of phase with the microwave field so that at the field maxima in either direction the electron is positioned as shown in Fig. 2. As in the case of circular polarization there are many stable states with $\mu$ oscillating both in and out of phase with $E$, and they are completely analogous to the Trojan and anti-Trojan wave packets discussed above.

## III. EXPERIMENTAL APPROACH

The essential notion of the experiment is easily understood with the help of the timing diagram of Fig. 3 and the

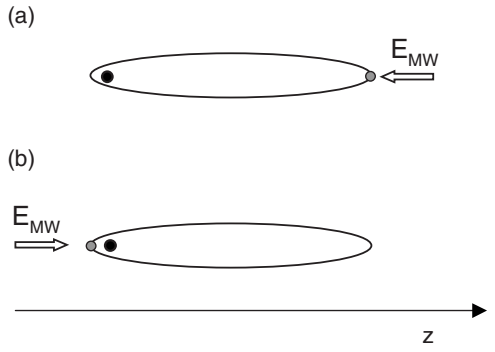


FIG. 2. One-dimensional atom subjected to the linearly polarized microwave field when its electron is (a) at the outer turning point and (b) at the inner turning point.

schematic diagram of Fig. 4. A thermal Li atomic beam passes between two capacitor plates 19 mm apart where the atoms are excited to Li $np$ states of $n \approx 70$ by three ns dye-laser pulses via the route

$$2s \rightarrow 2p \rightarrow 3s \rightarrow np,$$

which requires wavelengths of 670, 820, and 615 nm. The laser pulses are each 5 ns long, and the set of three pulses spans 20 ns. The dye lasers are pumped by the first Nd:YAG (yttrium aluminum garnet) laser, which runs at a 20 Hz repetition rate and sets the repetition rate for the experiment.

Approximately 100 ns after laser excitation the atoms are exposed to a microwave pulse from the horn shown in Fig. 4. The microwave pulse has a frequency in the vicinity of 17 GHz, is turned on in 10 ns, and has constant amplitude until it is turned off 0.1 – 3.1 $\mu$s later. The typical microwave-field amplitude is 1 V/cm, which is much smaller than the scaled Coulomb field $1/n^4 = 1/70^4 = 214$ V/cm.

The microwave field converts the atoms in the $np$ state into a nondispersing wave packet in which the electron's motion is synchronous with the microwave field, as shown in Fig. 2. We detect that the conversion to a synchronous wave packet has occurred by measuring the time-resolved momenta of the atoms with a half-cycle field pulse (HCP) [22,23] synchronized to the microwave field. The HCP preferentially ionizes atoms in which the electron is moving in the direction of the impulse from the HCP. After the end of

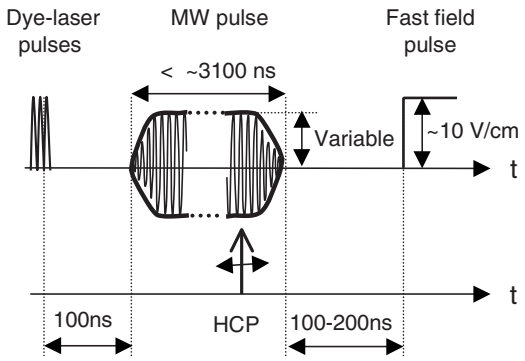


FIG. 3. A timing diagram of the experiment.

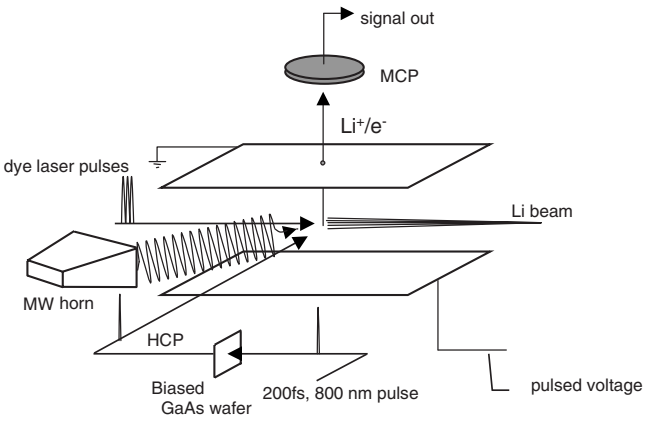


FIG. 4. A schematic diagram of the experimental setup.

the microwave pulse we usually apply a positive voltage pulse to the lower capacitor plate producing a field of ~10 V/cm, which drives ions formed by the HCP, through a ~900-$\mu$m-diam hole in the upper plate to a dual microchannel plate (MCP) detector. In some cases we apply a negative pulse of a few hundred volts to the lower plate after the microwave pulse to field ionize [24] those atoms not ionized by the HCP and drive the electrons produced through the hole in the upper plate to the MCP. In either case the signal from the detector is captured with a gated integrator.

The principle of detecting the time-resolved momentum of an electron in a highly elliptical, almost linear orbit using the HCP is shown in Fig. 5. The HCP gives the electron with initial momentum $p_0$ an impulsive momentum kick $\Delta p$, which changes the energy of the electron by

$$\Delta W = \overline{\Delta p} \cdot \overline{p_0} + \overline{\Delta p}^2/2. \tag{7}$$

If the energy transfer $\Delta W$ exceeds the initial binding energy the electron is ejected from the atom. From Eq. (7) it is apparent that $\Delta W$ can be positive or negative depending upon the relative orientation of $\Delta p$ and $p_0$, that is, the sign of $\Delta p \cdot p_0$. Along the bottom of the orbit (1 in Fig. 5), $\Delta p \cdot p_0 > 0$, and along the top (2 in Fig. 5), $\Delta p \cdot p_0 < 0$. When the amplitude of the HCP is set to ionize half the atoms, it will ionize atoms at the outer turning points, where $p_0 = 0$ and along 1 in Fig. 5, when the electron is moving to the right, in the direction of $\Delta p$.

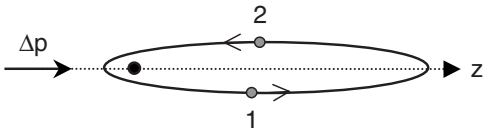


FIG. 5. The HCP, short compared to the orbital period, gives the electron a momentum kick $\Delta p$. Along the outgoing part of the orbit (at 1), $\Delta p$ adds to the electron's original momentum $p_0$ and the electron gains energy. Along the incoming part of the orbit (at 2), $\Delta p$ subtracts from the electron's initial momentum $p_0$ and the electron's energy can be reduced. Ionization occurs if the energy gain from the HCP exceeds the initial binding energy, and it is more likely to occur than the electron is on the outgoing part of the orbit.

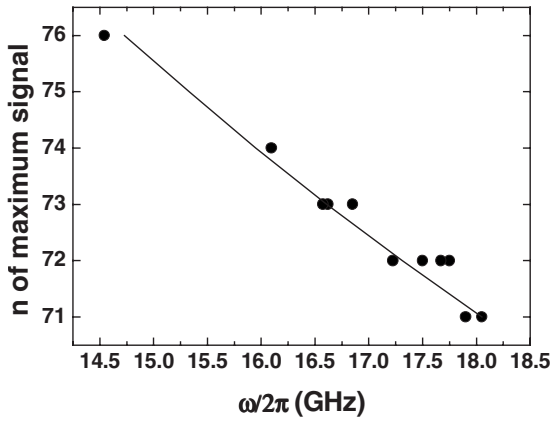


FIG. 6. Location of $n$ with the maximum signal vs microwave frequency (●). Also plotted in the figure is the Kepler frequency $\omega/2\pi=1/2\pi n^3$ (—).

The HCP is generated when a 200 fs, 800 nm laser pulse strikes a biased GaAs wafer in the vacuum system. The laser pulse creates conduction electrons, which are accelerated by the bias voltage and radiate a freely propagating HCP of 0.5 ps duration. There is a long weak tail of the opposite polarity [22], but its effect is minimal in this application, and we ignore it. With a bias voltage of ~500 V we ionize 50% of the atoms in the $n=72$ state. The 800 nm laser pulse is from a continuous-wave mode-locked Ti:sapphire laser, which produces a 76 MHz pulse train. Single pulses are amplified at a 20 Hz repetition rate with a regenerative amplifier pumped by a second Nd:YAG laser, and the resulting light pulse, typically attenuated to 0.15 mJ by a neutral density filter, is sent through an optical-delay stage to the GaAs wafer.

The HCP is synchronized with the microwave field by phase locking the microwave oscillator, a Hewlett Packard 8350B/E3550A sweep oscillator, to a harmonic of the 76 MHz repetition rate of the mode-locked Ti sapphire oscillator. We detect the 76 MHz pulse train from the laser with a New Focus ultrafast photodiode, which produces a frequency comb of harmonics of 76 MHz extending to 20 GHz. We mix the output of the sweep oscillator with the photodiode signal in a Watkins Johnson M86C double-balanced mixer to produce a difference-frequency signal, which we amplify by a factor of 20 and send to the frequency-modulation (FM) input of the sweep oscillator. When the sweep oscillator is tuned to within 0.6 MHz of a harmonic of 76 MHz the oscillator acquires phase lock to the photodiode signal. By measuring the wave form of the microwave with a Tektronix 11801C digital sampling oscilloscope with a SD-26 sampling head we determine the time jitter of the microwave field relative to the fs laser pulse to be ±5 ps, or ±15 degrees of phase at 17 GHz.

The phase-locked cw microwave output of the oscillator (~10 mW), is formed into pulses from 0.1- to 3.1-$\mu$s-long with a mixer or switch and is amplified with Miteq MPN4-02001800-23P and Hughes 8020H amplifiers before passing through a low-$Q$ Fabry-Pérot filter, to remove broadband noise, on its way to the horn in the vacuum system.

The temporal position of the HCP in the microwave pulse is controlled coarsely by adjusting the time the first Nd:YAG laser fires relative to the second, producing a coarse-timing uncertainty of 4 ns, that is, we know the location of the HCP within the microwave envelope to 4 ns. The fine adjustment of the HCP timing is made by adjusting the optical delay line of the f.s.-laser pulse, and the uncertainty in this delay time is 5 ps from the uncertainty in phase locking of the microwave oscillator. With the fine adjustment we can delay the HCP by up to ~300 ps, equivalent to five microwave periods at 17 GHz.

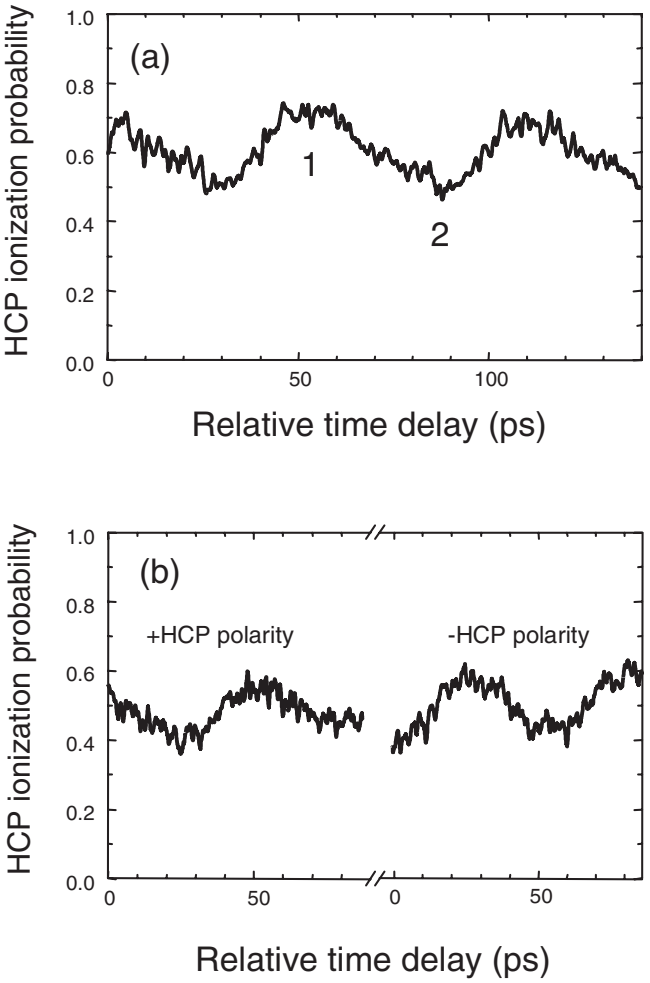


FIG. 7. Ionization probability vs fine delay time of the HCP 100 ns after the beginning of the 17.5 GHz, 1 V/cm microwave pulse: (a) HCP amplitude set to ionize ~60% of the atoms; (b) HCP with amplitude set to ionize ~50% of the atoms with the same polarity as (a) and reversed polarity. In all cases the modulation with period 56 ps indicates that the wave packet is phase locked to the microwave field. In (b) the phase of the signal reverses with HCP polarity as expected.

## IV. OBSERVATIONS

In the presence of a microwave field near the Kepler frequency we observe a clear variation in the ionization produced by the HCP as we delay the HCP relative to the microwave field. In Fig. 7 we show the ionization signal observed when atoms initially excited to the 72$p$ state are

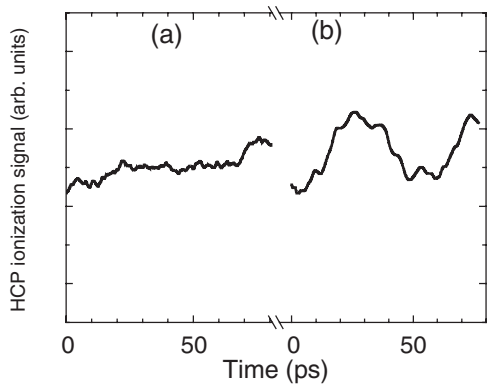


FIG. 8. HCP ionization signal of $n=72$ atoms with HCP of (a) horizontal and (b) vertical polarizations.

exposed to a 1 V/cm, 17.501 GHz linearly polarized microwave field. The HCP is polarized vertically up, and the coarse timing of the HCP is 100 ns after the start of the microwave pulse. Figure 7(a) shows the result of scanning the fine delay. The variation in the signal with a 57 ps period shows clearly that the electron's motion is synchronous with the microwave field. When the ionization signal is higher (1 in Fig. 7), the electron is moving in the same direction as $\Delta p$ and when it is lower [2 in Fig. 7(a)], the electron is moving in the direction opposite to $\Delta p$ (see Fig. 5).

If we change the microwave frequency we observe the maximum signal at a different $n$, corresponding to the resonance condition $1/n^3=\omega$. Specifically, as the microwave frequency is changed from 18 to 14.5 GHz the maximum signal moves from $n=71$ to $n=76$ (see Fig. 6). If we reverse the bias on the GaAs wafer we reverse the polarity of the HCP, and doing so reverses the sign of the variation in the HCP ionization signal, as shown in Fig. 7(b). If we rotate the GaAs wafer by 90° we can polarize the HCP perpendicular to the microwave field, and in this case we observe a variation in the HCP ionization signal roughly a factor of 10 smaller, as shown by Fig. 8. This measurement suggests that the electron's motion in the presence of the microwave field is approximately one dimensional.

The data shown in Figs. 7 and 8 were taken with $n$ chosen so that the $\Delta n=1$ transition frequency matches the microwave frequency. For 17.5 GHz, $n=72$ and $n=73$ are resonant. As the $n$ of the initially populated state is moved away from the resonant $n$ we observe the signals shown in Fig. 9 with 17.5 GHz microwave fields of 1 and 2 V/cm. While the absolute phase is arbitrary, the relative phases of all the traces in Figs. 9(a) and 9(b) are the same. In Fig. 9(a) we observe a signal that varies as $\cos \omega t$ for $n=72$ and 73, a nearly zero signal for $n=71$ and 74, and a phase-reversed signal that varies as $-\cos \omega t$ for $n<71$ and $n>74$. The phase reversal away from resonance is also observed with a 2 V/cm microwave field, as shown by Fig. 9(b). In this case the $70 \leqslant n \leqslant 75$ signals have a $\cos \omega t$ dependence, the $n=69$ and 76 signals have no variation, and, though it is a little obscure because of a smaller signal-to-noise ratio in this figure, the $n<69$ and $n>76$ signals have a $-\cos \omega t$ dependence. The aspect of Figs. 9(a) and 9(b), which was initially surprising, is the phase-reversal off resonance. The reversal

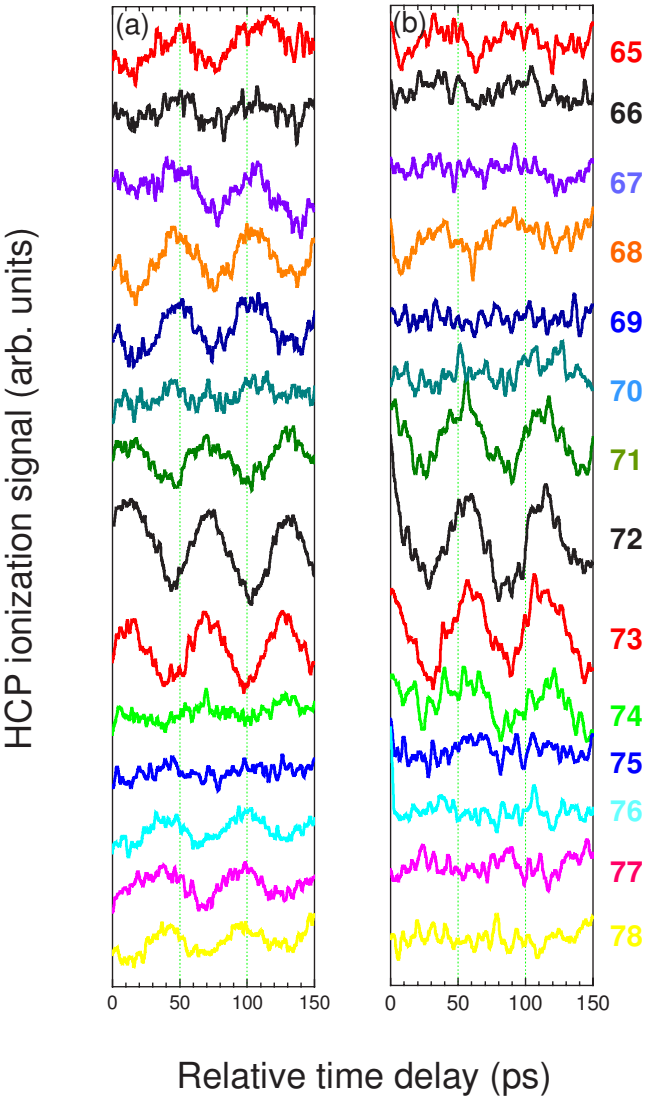


FIG. 9. (Color online) HCP ionization signals of atoms in the different initial $n$ at (a) $E=1$ V/cm and (b) $E=2$ V/cm.

is shown explicitly in Fig. 10, which is a plot of the amplitudes of the HCP ionization signals vs $n$ for a microwave field amplitude of 1 V/cm.

We have described observations made with the timing sequence of Fig. 3. The laser excitation can also be done during the microwave pulse, in which case we observe qualitatively similar results but with a smaller variation in the HCP signal with delay. To be more precise, the amplitudes of the signals are reduced by a factor of approximately two.

The data shown in Fig. 7 were taken 100 ns after the beginning of the microwave pulse, and at this point the wave packet has already lived a thousand times longer than a normal radial Rydberg wave packet. However, the wave packets are much longer lived than 100 ns. In Fig. 11 we show the HCP ionization probability for atoms initially excited to the $72p$ state and exposed to a 1 V/cm 17.5 GHz microwave field. There is no obvious difference between the coarse delays of 100 ns and 3.1 $\mu$s, and for times beyond 3.1 $\mu$s the atoms begin passing out of the field of view. These wave packets appear to be "eternal," as suggested by Buchleitner

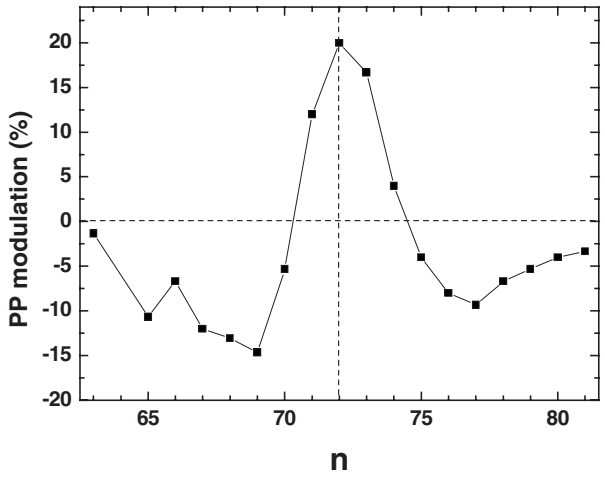


FIG. 10. Observed signal amplitudes with a 1 V/cm, 17.5 GHz field vs $n$. This frequency is resonant with $n=72$ and 73. The phase reversal of the signal far off-resonance is apparent.

and Delande [21], and they are apparently immune to dephasing.

## V. COMPARISON BETWEEN THEORY AND EXPERIMENT

It is instructive to compare the results of our experiments to one-dimensional models. As we shall see, the models contain most of the phenomena we observe. The quantum description of nondispersing wave packets is a Floquet picture [25–27], which is based upon the fact that the perturbation by the microwave field is periodic [21]. The solutions to the Schrödinger equation (the Floquet eigenstates) are assumed to have the same period.

The Hamiltonian $H$ is given by

$$H = H_0 + H'(t), \tag{8}$$

where

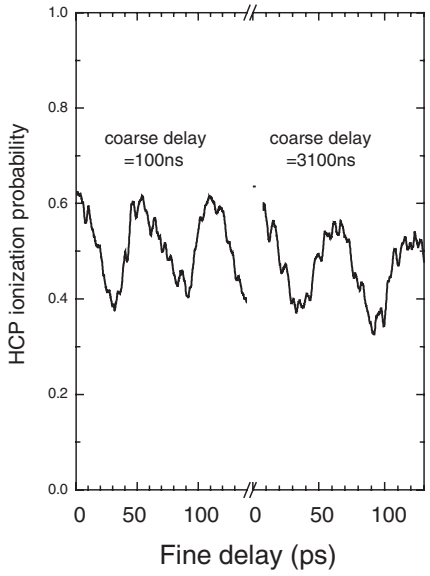


FIG. 11. HCP ionization signal for 100 and 3100 ns coarse delays.

$$H_0 = p^2/2 - 1/z, \tag{9}$$

and

$$H'(t) = zE\cos\omega t. \tag{10}$$

Here $p$ is the electron's momentum in the $z$ direction, and the microwave field in the $z$ direction is $E\cos\omega t$. The solutions to the Schrödinger equation,

$$i\frac{\partial\Psi(z,t)}{\partial t} = H(t)\Psi(z,t), \tag{11}$$

in the absence of the microwave perturbation are given by the energies and eigenfunctions of Eqs. (1) and (2), i.e.,

$$H_0|\phi_n(z)\rangle = \omega_n|\phi_n(z)\rangle, \tag{12}$$

where $\omega_n$ are the unperturbed energies [$\equiv W_n$ in Eq. (1)].

The perturbation $H'(t)$ couples different $n$ states, and we retain only the strongest of these couplings, the $\Delta n=1$ coupling, which is given by [18]

$$\langle\phi_n|z|\phi_{n+1}\rangle = 0.3n^2. \tag{13}$$

With $H'(t)$ the state vector $|\Psi(z,t)\rangle$, which satisfies the Schrödinger equation, can be written as

$$|\Psi(z,t)\rangle = \sum_{n'} T_{n'}(t)|\phi_{n'}(z)\rangle. \tag{14}$$

If, as in our case, $H'(t)$ is periodic, we can expand the wave function in a Fourier series, and

$$T_{n'}(t) = e^{-i\epsilon t}\sum_k A_{n',k}e^{-ik\omega t}, \tag{15}$$

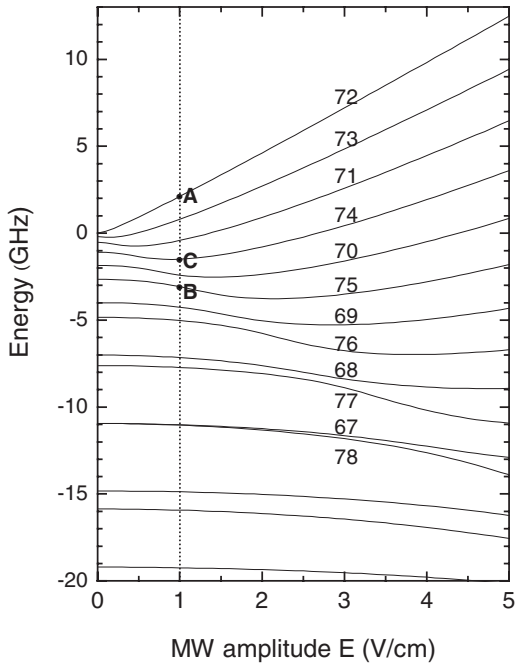


FIG. 12. Floquet-energy diagram vs 17.5 GHz microwave-field amplitude $E$. The energies are plotted relative to the energy of the $n=72$ state. Labels indicate the $n$ state adiabatically connected to each Floquet state.

where $\epsilon$ is a Floquet eigenenergy, $k$ is the number of microwave photons added to the internal energy of the atom, and $A$ is a coefficient. When Eq. (14) is substituted into the Schrödinger equation and the result is multiplied by $\langle \psi_n(z)|$ we obtain

$$i\frac{d}{dt}T_n(t) = \omega_n T_n(t) + E(t)\sum_{n'} T_{n'}(t)\langle \phi_n(z)|z|\phi_{n'}(z)\rangle, \quad (16)$$

in which $E(t)=E\cos\omega t$. Using the explicit form for $T_{n'}(t)$ of Eq. (15) we can write Eq. (16) in the time-independent form,

$$(\omega_n - k\omega)A_{n,k} + \sum_{n'} V_{n,n'}(A_{n',k+1} + A_{n',k-1}) = \epsilon A_{n,k}, \quad (17)$$

where

$$V_{n,n'} = \frac{E}{2}\langle \phi_n(z)|z|\phi_{n'}(z)\rangle. \quad (18)$$

Since we have disregarded the $|\Delta n| > 1$ matrix elements, the only off-diagonal elements are

$$V_{n,n+1} = 0.15En^2. \quad (19)$$

We diagonalize the Floquet-Hamiltonian matrix to find the Floquet eigenvectors and eigenvalues. The matrix is infinite, but it can be broken into nearly degenerate blocks. In particular, we consider the block of states nearly degenerate with the $n=72$ state. These are states with zero-field Floquet energies of $\omega_{72}$, $\omega_{73}-\omega$, $\omega_{74}-2\omega$, $\omega_{71}+\omega$, $\omega_{70}+2\omega,\ldots$, This restriction, which corresponds to the rotating-wave approximation, is reasonable as long as the spacings between the Floquet states are small compared to the microwave frequency. Since we only consider the $\Delta n=1$ dipole-matrix elements, the central block of the Floquet-Hamiltonian matrix $H_F$ has the tridiagonal form,

$$H_F = \begin{pmatrix} \cdot & \cdot & & & & & & \\ \cdot & \omega_{70}+2\omega & f_{70} & & & & & \\ & f_{70} & \omega_{71}+\omega & f_{71} & & & & \\ & & f_{71} & \omega_{72} & f_{72} & & & \\ & & & f_{72} & \omega_{73}-\omega & f_{73} & & \\ & & & & f_{73} & \omega_{74}-2\omega & \cdot & \\ & & & & & \cdot & \cdot & \end{pmatrix}, \quad (20)$$

where $f_n \equiv V_{n,n+1}$.

Diagonalizing the matrix of Eq. (20) for 17.5 GHz microwave-field amplitudes from 0 to 5 V/cm gives the Floquet-energy eigenvalues plotted in Fig. 12. At zero field the Floquet energies are $\omega_n-(n-72)\omega$, and the states for which $\omega$ is closest to the $\Delta n=1$ frequency lie highest in energy. As the field is raised from zero the pattern is qualitatively like the Stark structure of a nonhydrogenic atom. The highest-lying, near-resonant states are split into states with large Stark shifts at quite low fields, and as the field is raised lower-lying states, which are further from resonance, begin to exhibit obvious Stark shifts.

The slopes of the energy levels $dW/dE|_E$ are twice their dipole moments at the field amplitude $E$. The rotating-wave approximation introduces the factor of one half. The dipoles oscillate synchronously with the microwave field. For example, at 1 V/cm the state at $A$ in Fig. 12 has a dipole moment antiparallel to $E$ while the state $B$ has a dipole moment parallel to $E$, and the state $C$ has no dipole moment. The fact that the dipoles oscillate can be observed explicitly in the time evolution of $|\Psi(z,t)|^2$. In Fig. 13(a) we show the time evolution of the probability distribution of the highest-energy Floquet state, which is adiabatically connected to the zero-field $n=72$ state, at a microwave-field amplitude of 1 V/cm. Specifically, we show when $\omega t=0,\pi/2,\pi$, and $3\pi/2$. It is quite evident that the probability moves from large $z$ at $\omega t=0$ to small $z$ at $\omega t=\pi$. In contrast, the Floquet state connected to the zero-field $n=75$ state exhibits an oscillation with reversed phase, as shown in Fig. 13(b). At $\omega t=0$ the electron is at small $z$ while at $\omega t=\pi$ it is at large $z$. Where states have vanishing Stark shifts they exhibit little change in the average radial position as $\omega t$ changes from 0 to $2\pi$. Both the Floquet energy-level diagram of Fig. 12 and the time dependences shown in Fig. 13 are consistent with the phase reversals of Figs. 9 and 10.

In the experiment the atoms are usually excited in zero field, after which the microwave field is turned on in $\sim$10 ns. With this turn-on time the atoms should pass adiabatically from zero field to the steady-state amplitude of the microwave pulse. If the steady-state field amplitude is 1 V/cm an atom initially in the $n=72$ state goes to point $A$ of Fig. 12, where $\mu$ is antiparallel to $E$; an atom in $n=74$ goes to point $C$ where there is a smaller dipole, and an atom initially in $n<71$ or $n>74$ goes to points where $\mu$ is parallel to $E$. Thus the HCP ionization signals for $n<71$ and $n>74$ should be reversed in phase relative to the $n=72$ signal, and the $n=71$ signal should be vanishingly small, which is in qualitative agreement with the experimental observations of Figs. 9 and 10. When the laser excitation occurs in the microwave field the amplitude of the HCP is reduced, presumably be-

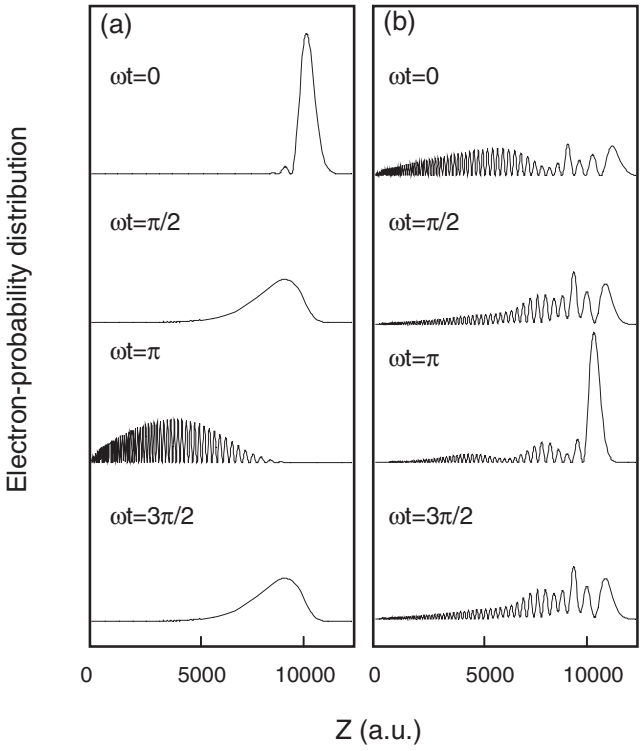


FIG. 13. Electron-probability distribution of the nondispersing wave packet at the microwave phase of 0, $\pi/2$, $\pi$, and $3/2\pi$ when microwave-field amplitude $E=1$ V/cm. Plots show for (a) the highest-energy Floquet state, which is adiabatically connected to the zero-field $n=72$ state and (b) the Floquet state connected to the zero-field $n=75$ state. The former has a large time-varying dipole while the latter does not.

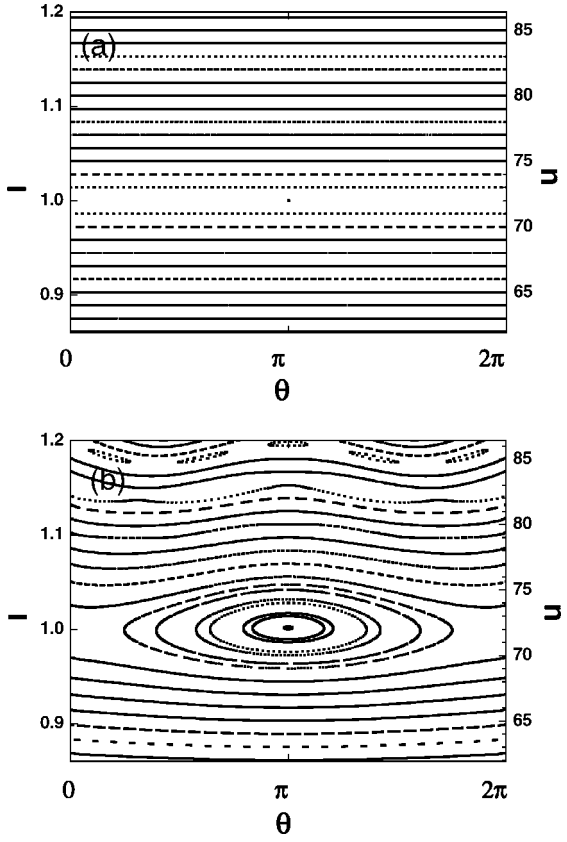


FIG. 14. $(I,\theta)$ phase-space plot of the one-dimensional H atom in resonance 17.628 GHz microwave field plotted when (a) microwave-field amplitude $E=0$ V/cm and (b) $E=1$ V/cm. Each curve is calculated by starting an atom in a different initial $n$ ($60 \leqslant n \leqslant 89$) with its electron at the outer turning point and subjecting it to the 320 cycle microwave-field pulse. The scale of the right axis in the figures corresponds to the value of $I$ in zero field, i.e., $n$.

cause we are making more than one Floquet state.

Nondispersing wave packets can also be described using classical mechanics. The standard approach is to integrate the equation of motion and find the stable orbits. For a one-dimensional atom the Hamiltonian is expressed in Eqs. (8)–(10), and the results are usually displayed as Poincaré surfaces of section using action-angle variables $(I,\theta)$ [27,28]. For our one-dimensional atom $I$ and $\theta$ are defined by

$$I=\frac{1}{2\pi}\oint p dz \tag{21}$$

and

$$\theta=\begin{cases}\eta-\sin\eta & p\geqslant 0\\ 2\pi-\eta+\sin\eta & p<0,\end{cases} \tag{22}$$

where $\eta=2\sin^{-1}(z/2n^2)$, $\theta$ is the eccentric anomaly, and in the absence of a microwave field $I=n$, the principal quantum number.

It is convenient to use $\theta$ rather than $z$ since it increases linearly with time in the absence of a microwave field. For our purposes it is convenient to note that at $\theta=\pi$ the electron is at the outer turning point $z=2n^2$, and at $\theta=0$ and $2\pi$ the electron is at the inner turning point of its orbit, $z=0$.

The surfaces of section are generated by integrating the equation of motion and plotting the values of $I$ and $\theta$ after each cycle of the perturbation, in our experiment a 17.5 GHz microwave field, slightly off-resonance to the $n=72-73$ transition frequency, 17.628 GHz. Here we omit the small quantum defect (~0.05) of Li $np$ states and use a hydrogenic value. Before presenting the result in the presence of a field it is useful to imagine the result in the resonance field with 0 V/cm, i.e., no field. If the initial action leads to an orbit with a 17.628 GHz Kepler frequency, on each successive cycle of the field the same values of $I=I_0$ and $\theta=\theta_0$ will be found, and the surface of section is a point, as shown in Fig. 14(a) for $n=72$. In all cases shown in Fig. 14 the initial condition is $\theta_0=\pi$, i.e., the electron is at the outer turning point of its orbit. Choosing different values of $\theta_0$ will lead to different points along $I=I_0$, but the result is always a point. For any other choice of $I_0$—one not having a Kepler frequency of 17.628 GHz—on successive cycles $\theta\neq\theta_0$, although $I=I_0$, with the result that the surface of section is a horizontal line, as shown in Fig. 14(a). $\theta$ changes but $I$ does not since the constant energy only depends on $I$. The essential point is that when the initial conditions are such that the electron's motion is resonant with the (vanishing) microwave field the surface of section generated from any starting point is that point. For any nonresonant initial conditions it is a horizontal line.

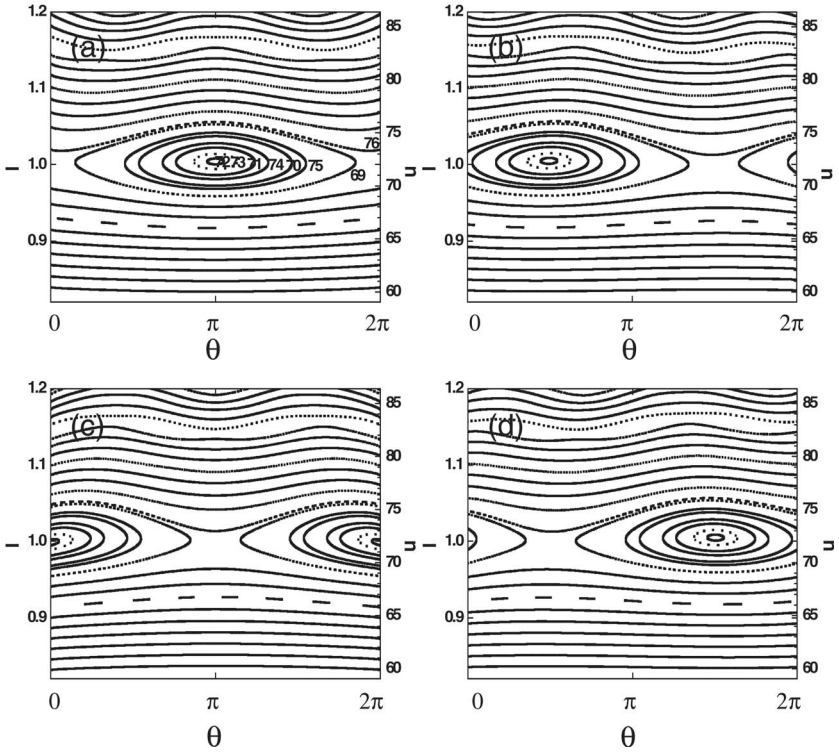


FIG. 15. $(I,\theta)$ phase-space plot of the one-dimensional atom in 1 V/cm, 17.5 GHz microwave field plotted when (a) $2\pi\omega t=j$, (b) $2\pi\omega t=(j+1/4)$, (c) $2\pi\omega t=(j+1/2)$, and (b) $2\pi\omega t=(j+3/4)$, where $j=0,1,2,\ldots$. Each curve is calculated for an atom in a different initial $n$ $(60\leqslant n\leqslant 89)$ with its electron at the outer turning point and subjected to the 320 cycle microwave-field pulse. The scale of the right axis in the figures corresponds to the value of $I$ in zero field, i.e., $n$.

Now we apply a microwave field $E\cos\omega t$ and examine the surface of section at $\omega t=2\pi j$, where $j$ is an integer, i.e., at the peak microwave field. In Fig. 14(b) we show the result for a 1 V/cm, 17.628 GHz field. For $n\leqslant 70$ and $n\geqslant 74$, far from the resonance, the surfaces of section are distorted lines, indicating slightly perturbed orbits. There is a nonlinear resonance island in which the electron does not sample all $\theta$ (or $z$). The island has grown from the single stationary point in the zero-field case to a finite-sized island. Now even if the electron initially has a nonresonant action it is often found near $\theta=\pi$, i.e., at large $z$ when the microwave electric field is in the $+z$ direction, as shown in Fig. 2. If the initial action is nearly resonant, e.g., $n=72$ the surface of section is a small oval indicating that the electron's motion oscillates between slightly leading and slightly lagging the microwave field. In all cases $\theta\approx\pi$, or $z\sim 2n^2$ at the peak of the microwave field. As the initial condition becomes further removed from resonance the oval becomes larger, indicating that the oscillation in the lead or lag phase is becoming larger. While the average value of $\theta$ is $\pi$, for only a small fraction of the orbits is $\theta\approx\pi$.

The surface of section of Fig. 14 is plotted at $\omega t=2\pi j$ $(j=0,1,2,\ldots)$ with $j$ up to 320, i.e., 320 microwave cycles. If we start with the same field and initial conditions but the microwave field of 17.5 GHz, we find the results shown in Fig. 15, in which we plot the surfaces of section at (a) $\omega t=2\pi j$, (b) $\omega t=2\pi(j+1/4)$, (c) $\omega t=2\pi(j+1/2)$, and (d) $\omega t=2\pi(j+3/4)$, where $j=0,1,2,\ldots,320$. It is apparent that when $\omega t=2\pi(j+1/4)$ the resonance island moves and is centered at $\theta\approx\pi/2$, or $z\sim 9100$, and when $\omega t=2\pi(j+1/2)$ the center of the resonance island is at $\theta=\pi$ or $z=0$. The center of the resonance island moves synchronously with the microwave field, and the atomic dipole is antiparallel to the microwave field. In other words, the center of the resonance island corresponds to the highest-energy Floquet state of Fig. 12.

At the edge of the resonance island, $n=69$ or $n=75$, the electron's orbit is, on average synchronous with the microwave field, but there are large oscillations in the phase by which it leads or lags the microwave field. As with all oscillations, most of the time is spent at the turning points, and this phenomenon can be seen in the density of points in Fig. 15. For the $n=69$ orbit of Fig. 15(a) it is apparent that the highest density of points is at $\theta\approx\pi/6$ and $2\pi-\pi/6$ or $z\sim 5000$, i.e., small $z$. Using Eq. (22) we can convert the density of points along the orbit into a spatial-probability distribution, and in Fig. 16 we show the spatial-probability distributions corresponding to $n=72$ and $n=69$ of Fig. 15 at $\omega t=2\pi j$, $2\pi(j+1/4)$, and $2\pi(j+1/2)$. As shown by Fig. 16 the $z$-probability distributions oscillate out of phase in these two cases, with the dipole in the $n=69$ case, the edge of the resonance island, oscillating in phase with the microwave field. It is thus apparent that the edge of the resonance island corresponds to the downward-shifted Floquet states of Fig. 12.

An interesting question is why nondispersing wave packets maintain their localization so much longer than normal radial wave packets. For example, consider the classical orbit shown in Fig. 17. A normal wave packet following this orbit, composed of the $\phi_n$ eigenstates of energies $W_n$, is represented at any time $t$ by Eq. (3), in which the coefficients $a_n$ and energies $W_n$ are constant. The only difference between the wave packet when it is localized at points $A$ and $B$ is in the phases; the energies are the same. Thus at the same time a wave packet can be localized at $A$ or $B$ and have the same energy simply by changing the phases by an amount of order $\pi$. Consequently, when these phases accumulate errors of order $\pi$ the localization of the wave packet is destroyed. In a 1 $\mu$s observation time such phase shifts correspond to only

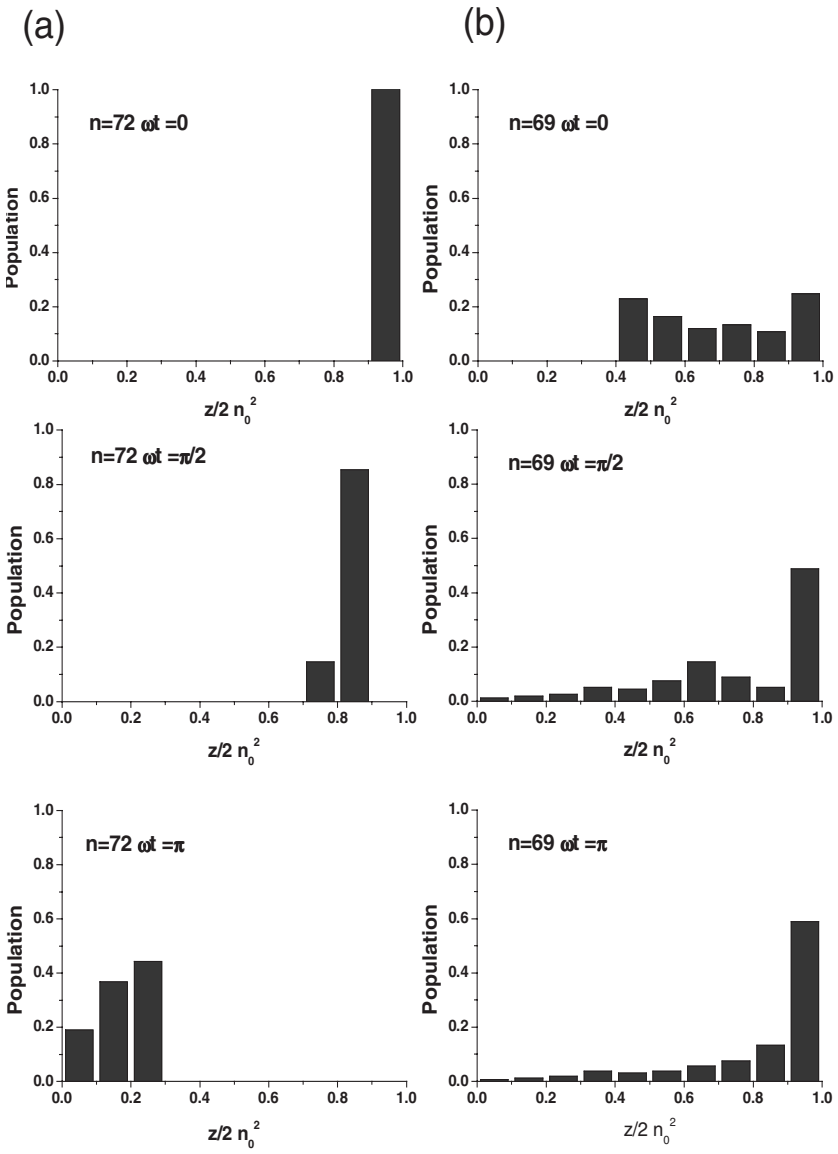


FIG. 16. Probability distribution generated from the density of points in the surface of sections for (a) $n=72$ and (b) $n=69$ for microwave phases of $\omega t=0$, $\omega t=\pi/2$, and $\omega t=\pi$. Plots are made by taking a histogram of phase-space plot of $n=72$ and $n=69$ atoms subjected to 1 V/cm, 17.5 GHz, 160 cycle microwave-field pulse.

1 MHz relative frequency shifts of the levels.

In the nondispersing wave packet it is no longer true that the energy of the wave packet is the same if the electron is at point $A$ or point $B$ at the same time, due to the presence of the microwave field. If, for example, the microwave field points to the right, having the electron at point $A$ is a lower-energy state than having it at point $B$. The energy difference, averaged over a microwave cycle is the difference between the up- and down-shifted Floquet states of Fig. 17. Now a frequency change of order hundreds of MHz is required to destroy the localization of the wave packet; it is no longer free.

## VI. CONCLUSION

We have reported the observation of nondispersing wave packets created with the aid of a weak microwave field, which not only overcomes the delocalizing effect of the dispersion in the energy-level spacings but makes the wave packets orders of magnitude more immune to other forms of dephasing. The results of our observations can be explained in a straightforward way by both quantum and classical models. In spite of the fact that the models are based on one-dimensional motion of the electron they give reasonably good pictures of the underlying physics.

There are still many open questions. For example, what are the effects of stray fields? How many subtle details are

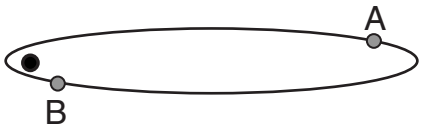


FIG. 17. In a normal wave packet there is no difference in energy between the cases in which the electron is at points $A$ and $B$, near the outer and inner turning points. Consequently, the localization of such wave packets is easily destroyed by small phase shifts of the constituent states. In a nondispersing wave packet in a microwave field there is an energy difference between the electron's being at points $A$ and $B$ at any given time, and these wave packets are much more unlikely to be delocalized.

obscured by the fact that the atoms are not one dimensional? Can nondispersing wave packets be made as easily in an atom or molecule having several quantum defects ~1? In Li only the *s* states have a quantum defect larger than 0.05. Finally, what are the effects of perturbations and noise on these wave packets?

In addition to their intrinsic interest nondispersing Rydberg wave packets may be of some use. For example, the atoms in our wave packet all have synchronously oscillating dipole moments, and they could be used as targets in collision experiments. The oscillating dipole moments also raise the question of the relation of these wave packets to superradiance. Finally, since the nondispersing wave packet is a long-lived coherent superposition state, it could be of use for storing quantum information if Rydberg-atom gates [29] are used. It is a sort of decoherence-free subspace analogous to that used in ion traps [30].

## ACKNOWLEDGMENTS

It is a pleasure to acknowledge stimulating discussions with R. R. Jones, A. Buchleitner, F. B. Dunning, T. A. Miller, R. M. Field, and F. Merkt. This work has been supported by the National Science Foundation under Grant No. PHY-0555491.

[1] J. Mehra and H. Rechenberg, *The Historical Development of Quantum Theory* (Springer-Verlag, New York, 1982), Vol. 1, pp. 155-257.
[2] E. Schrödinger, *Collected Papers on Wave Mechanics* (Blackie & Son Ltd., London, 1928), p. 41.
[3] J. Mehra and H. Rechenberg, in *The Historical Development of Quantum Theory* (Springer-Verlag, New York, 1987), Vol. 5, pp. 633-636.
[4] L. S. Brown, Am. J. Phys. **41**, 525 (1973).
[5] J. Parker and C. R. Stroud, Jr., Phys. Rev. Lett. **56**, 716 (1986).
[6] G. Alber, H. Ritsch, and P. Zoller, Phys. Rev. A **34**, 1058 (1986).
[7] M. J. Rosker, T. S. Rose, and A. H. Zewail, Chem. Phys. Lett. **146**, 175 (1988).
[8] P. M. Felker, J. S. Baskin, and A. H. Zewail, J. Phys. Chem. **90**, 724 (1986).
[9] S. Haroche, in *High Resolution Laser Spectroscopy*, edited by K. Shimoda (Springer, Berlin, 1976).
[10] J. N. Dodd and G. W. Series, in *Progress in Atomic Spctroscopy*, edited by W. Hanle and H. Kleinpoppen (Plenum, New York, 1978).
[11] A. ten Wolde, L. D. Noordam, A. Lagendijk, and H. B. van Linden van den Heuvell, Phys. Rev. Lett. **61**, 2099 (1988).
[12] A. ten Wolde, L. D. Noordam, A. Lagendijk, and H. B. van Linden van den Heuvell, Phys. Rev. A **40**, 485 (1989).
[13] I. Bialynicki-Birula, M. Kalinski, and J. H. Eberly, Phys. Rev. Lett. **73**, 1777 (1994); *ibid.* **75**, 973 (1995).
[14] D. Farrelly, E. Lee, and T. Uzer, Phys. Rev. Lett. **75**, 972 (1995); Phys. Lett. A **204**, 359 (1995).
[15] E. Lee, A. F. Brunello, and D. Farrelly, Phys. Rev. Lett. **75**, 3641 (1995).
[16] H. Maeda and T. F. Gallagher, Phys. Rev. Lett. **92**, 133004 (2004).
[17] C. L. Stokely, F. B. Dunning, C. O. Reinhold, and A. K. Pattanayak, Phys. Rev. A **65**, 021405(R) (2002).
[18] H. A. Bethe and E. E. Salpeter, *Quantum Mechanics of One- and Two-Electron Atom* (Plenum, New York, 1977).
[19] J. A. Yeazell, M. Mallalieu, and C. R. Stroud, Jr., Phys. Rev. Lett. **64**, 2007 (1990).
[20] M. Kalinski and J. H. Eberly, Phys. Rev. Lett. **77**, 2420 (1996).
[21] A. Buchleitner and D. Delande, Phys. Rev. Lett. **75**, 1487 (1995); A. Buchleitner, Ph.D. thesis, Universite Pierre et Marie Curie, Paris VI, 1993 (unpublished).
[22] D. You, R. R. Jones, P. H. Bucksbaum, and D. R. Dykaar, Opt. Lett. **18**, 290 (1993).
[23] C. Raman, C. W. S. Conover, C. I. Sukenik, and P. H. Bucksbaum, Phys. Rev. Lett. **76**, 2436 (1996); R. R. Jones, *ibid.* **76**, 3927 (1996); C. O. Reinhold, J. Burgdörfer, M. T. Frey, and F. B. Dunning, Phys. Rev. A **54**, R33 (1996).
[24] T. F. Gallagher, *Rydberg Atoms*, (Cambridge Univ. Press, Cambridge, 1994).
[25] J. H. Shirley, Phys. Rev. **138**, B979 (1965).
[26] S. H. Autler and C. H. Townes, Phys. Rev. **100**, 703 (1955).
[27] A. Buchleitner, D. Delande, and J. Zakrzewski, Phys. Rep. **368**, 409 (2002).
[28] See, for example, R. V. Jensen, Phys. Rev. A **30**, 386 (1984); R. V. Jensen, S. M. Susskind, and M. M. Sanders, Phys. Rep. **201**, 1 (1991); J. Henkel and M. Holthaus, Phys. Rev. A **45**, 1978 (1992).
[29] D. Jaksch *et al.*, Phys. Rev. Lett. **85**, 2208 (2000).
[30] C. Langer *et al.*, Phys. Rev. Lett. **95**, 060502 (2005).